Green synthesis of Ba-Doped TiO2 nanoparticles using Blepharis maderaspatensis leaf extract for enhanced photocatalytic and antioxidant activities

Anbuvannan M
anbuphy85@gmail.com

Thiruvalluvar University

Maria Vinosel V
University of Madras

Rajesh S
Anna University, Chennai

Dhatshanamurthi P
Thiruvalluvar University

Karuppaiah Selvakumar
Saveetha Institute of Medical And Technical Sciences

Lakshmanan D
Thiruvalluvar University

Ramesh M
Mother Teresa Women's University

Aboud Ahmed Awadh Bahajjaj
King Saud University

Mohamed Ouladsmane
King Saud University

Research Article

Keywords: Green synthesis, Blepharis maderaspatensis, Ba-doped TiO2, Hydrothermal method, Photocatalytic degradation, DPPH, Antioxidant, High recyclability, Industrial applications

Posted Date: April 2nd, 2026

DOI: https://doi.org/10.21203/rs.3.rs-8786081/v1

Additional Declarations: No competing interests reported.

Version of Record: A version of this preprint was published at Journal of Materials Science: Materials in Electronics on July 1st, 2026. See the published version at https://doi.org/10.1007/s10854-026-17867-9.

Green Synthesis of Ba-Doped TiO_2 Nanoparticles using *Blepharis maderaspatensis* Leaf Extract for Enhanced Photocatalytic and Antioxidant Activities

M.Anbuvannan [a*], V. Maria Vinosel [b], S.Rajesh [c], P.Dhatshanamurthi [d], Karuppaiah Selvakumar [e], D.Lakshmanan [a], M.Ramesh [f], Aboud Ahmed Awadh Bahajjaj [g], Mohamed Ouladsmane [g]

[a]*Department of Physics, Thiruvalluvar University, Serkkadu, Vellore-632115, Tamil Nadu, India*

[b]*Department of Physics, Loyola College, University of Madras, Chennai -34, Tamil Nadu, India*

[c]*Department of Physics, GRT Institute of Engineering and Technology, Tiruttani-631209, Tamil Nadu, India*

[d]*Department of chemistry, Sun Arts and Science College, Tiruvannamalai-606755, Tamil Nadu, India*

[e]*Department of Physiology, Saveetha Dental College and Hospitals, Saveetha Institute of Medical and Technical Science (SIMATS), Saveetha University, Chennai -600077, India*

[f]*Department of Physics, M.V. Muthiah Government Arts College for Women, Dindigul-624 001, Tamil Nadu, India*

[g]*Department of Chemistry, P. O. Box 2455, College of Science, King Saud University, Riyadh 11451, Saudi Arabia*

*Corresponding author: anbuphy85@gmail.com (Dr.M.Anbuvannan)

Abstract

In this study, non-toxic and inexpensive biosynthesized Ba-doped TiO_2 nanoparticles were produced using chemical and green synthesis methods. In the green synthesis method, *Blepharis maderaspatensis* leaf extract was used as a natural stabilizing and reducing agent instead of chemical reagents.The biosynthesized TiO_2 nanoparticles were characterized using XRD, UV-DRS, FTIR, SEM, and TEM. The crystalline tetragonal structure, phase purity, and average crystallite size of 20-40nm. Methylene blue was used as a model organic pollutant to assess the photocatalytic performance of the produced samples under UV–visible light irradiation. Notably, the biosynthesized Ba-doped TiO_2 exhibited superior photocatalytic activity, achieving up to 96% degradation efficiency within 100 min, outperforming both chemically and biosynthesized nanoparticles. The DPPH assay was used to assess the antioxidant capacity of the biosynthesized TiO_2 nanoparticles. At a concentration of 80µg/mL, the DPPH radical scavenging activities were 74.80% and 76.57% DPPH radical scavenging respectively. The powerful antioxidant qualities of *Blepharis maderaspatensis* extract demonstrate its promise as a sustainable and environmentally friendly substitute for traditional synthesis methods.

Keywords: Green synthesis, *Blepharis maderaspatensis*, Ba-doped TiO_2, Hydrothermal method, Photocatalytic degradation, DPPH, Antioxidant, High recyclability, Industrial applications.

1 Introduction

Titanium dioxide (TiO_2) nanoparticles have attracted considerable attention owing to their outstanding physicochemical properties, including high chemical stability, non-toxicity, strong oxidative potential, and excellent photocatalytic activity [1–3]. Owing to these properties, TiO_2 is a viable option for various applications, including solar cells, medicinal devices, energy conversion, environmental cleanup, sensors, and cosmetics [4, 5]. Among the various TiO_2 polymorphs, the anatase phase, possessing a tetragonal crystal structure and a wide band gap of approximately 3.2–3.4 eV, is particularly favored for photocatalytic applications owing to its superior charge transport properties and higher surface reactivity [6-8]. Traditionally, physical and chemical techniques such as microwave [9], solvothermal hydrothermal sol–gel [10], solid-state [11], solution route [12], chemical phase breakdown [13], ultrasonic irradiation [14], and green synthesis methods are used to create TiO_2 nanoparticles. [15]. although these techniques offer substantial control over particle size and crystallinity, they often require high-energy inputs, toxic chemicals, and stringent reaction conditions, which limit their environmental sustainability and large-scale applicability. In recent years, green synthesis has emerged as a viable alternative, emphasizing the use of biological resources to produce nanomaterials in an eco-friendly, cost-effective, and scalable manner.

Plant-mediated synthesis has gained popularity because of the variety of bioactive substances that can simultaneously function as reducing, stabilizing, and capping agents, such as polyphenols, flavonoids, alkaloids, proteins, and carbohydrates. Using extracts from a variety of plant sources, such as *Catharanthus roseus* [16], *Psidium guajava* [17], *Mentha arvensis* [18], *Murraya koenigii* [19], *Musa AAA* and *Jatropha curcas L* [20], *Psidium guajava* [21], and *Tinospora cordifolia* [22], several studies have shown the successful green synthesis of TiO_2 nanoparticles, highlighting their potential for biological and environmental applications. Doping TiO_2 with alkaline earth or transition metal ions is an effective strategy for further enhancing its photocatalytic efficiency by modifying its electronic structure, suppressing electron–hole recombination, and improving light absorption. In this context, Ba incorporation into the TiO_2 lattice has attracted interest because of its ability to influence crystallite growth, surface defects, and charge carrier dynamics, thereby improving the photocatalytic performance. *Blepharis maderaspatensis* is a medicinal plant traditionally used to treat various ailments, including wounds, ulcers, headaches, and inflammation. The plant is rich in phytochemicals that can serve as natural reducing and stabilizing agents, making it an excellent candidate for synthesizing green nanomaterials. However, the utilization of *Blepharis maderaspatensis* leaf extract for the synthesis of Ba-doped TiO_2 nanoparticles and their photocatalytic applications remains relatively unexplored.

2. Materials and methods

2.1. Preparation of *Blepharis maderaspatensis* leaf extract

Fresh leaves of *Blepharis maderaspatensis* were collected from the Parvathamalai Hills in the Thiruvannamalai District of Tamil Nadu, India (12.4352° N, 78.9684° E). To remove dust and surface contaminants, the leaves were thoroughly cleaned several times using double-distilled water. In a 250 mL glass beaker, 10 g of finely chopped leaves were mixed with 100 mL of distilled water. The mixture was heated to 60°C with constant magnetic stirring for 30 min, during which time the color of the solution progressively changed from colorless to pale yellow, signifying the extraction of phytochemicals. Whatman No. 1 filter paper was used to filter the extract once it had cooled to room temperature, and the extract was stored for later use.

2.2. Green synthesis of TiO_2 and Ba-doped TiO_2 nanoparticles

To create the TiO_2 nanoparticles, 12.5 mL of titanium isopropoxide and 80 mL of 2-propanol were combined, and the mixture was magnetically agitated for 30 min at 60°C. To aid in the bioreduction and stability of TiO_2 nanoparticles, 20 mL of the produced leaf extract was added dropwise while being continuously stirred. For Ba doping, 0.0892g of Ba $(NO_3)_2$ was dissolved in 5mL of distilled water to create an aqueous solution of barium nitrate (0.01M). The reaction mixture was continually stirred while the barium precursor solution was gradually added. After allowing the resultant suspension to settle at room temperature, it was filtered through Whatman No. 1 filter paper and repeatedly cleaned with deionized water to remove any remaining contaminants. To increase the crystallinity of the precipitate, it was first dried in an oven at 100°C for five hours and then annealed at 700°C for two hours. The finished Ba-doped TiO_2 nanoparticles were collected and examined.

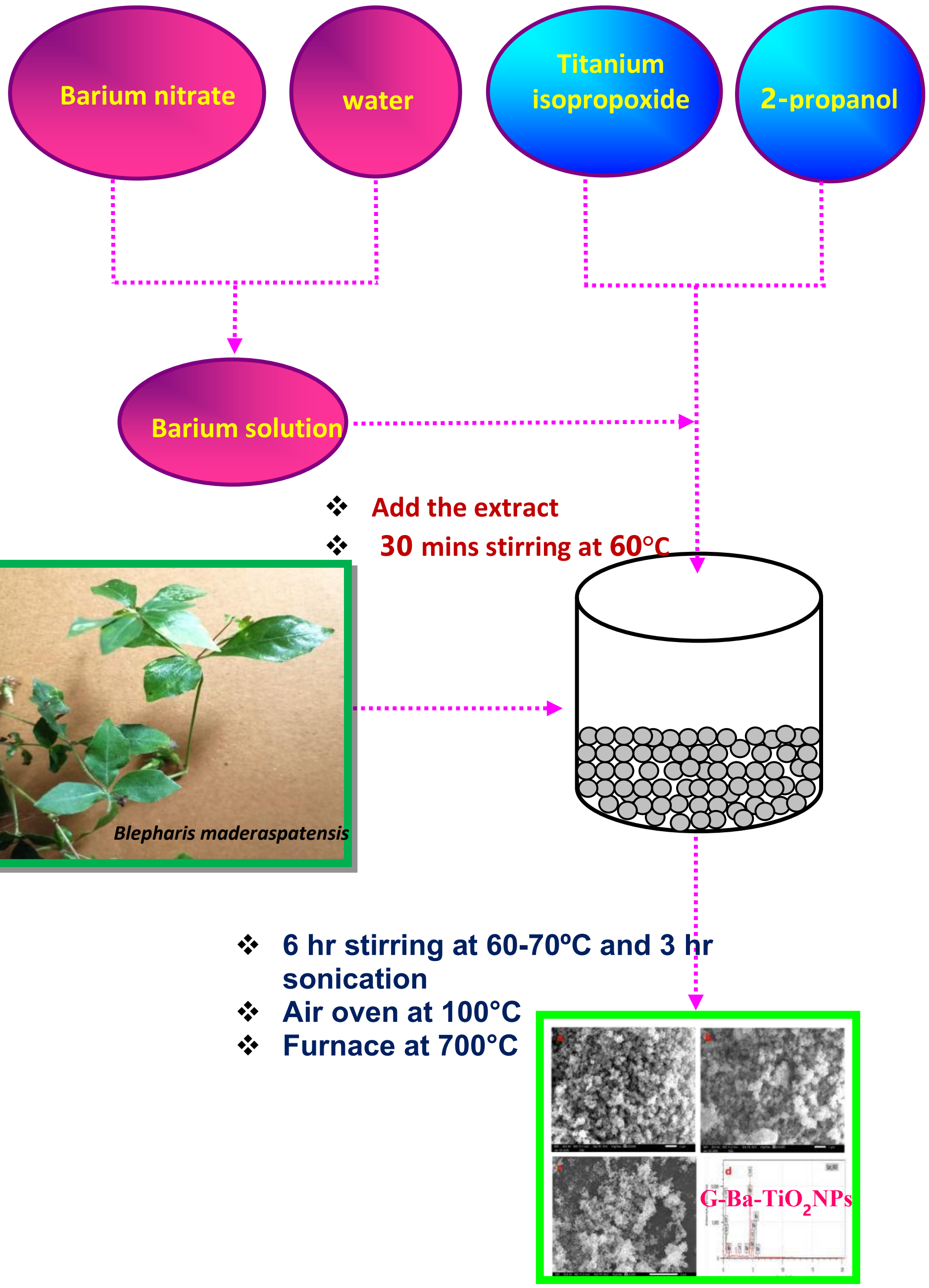

Fig. 1 Preparation of G-Ba doped TiO_2 nanoparticles

2.3 Photocatalytic degradation

Methylene blue (MB) was used as a model organic pollutant to assess the photocatalytic efficacy of the nanoparticles. To ensure equal dispersion, 50 mL of MB solution and 100 mg of the photocatalyst were combined in a 100 mL beaker and ultrasonicated for 20 min. To create an adsorption–desorption equilibrium, the suspension was left in the dark for 30 min before being exposed to light. Aliquots were taken at regular intervals of 30 min during the photodegradation studies, which were carried out under UV–visible light irradiation. A UV-visible spectrophotometer was used to measure the absorbance at 664 nm to track the concentration of MB.

2.4 Antioxidant activity

The DPPH free radical assay was used to evaluate the antioxidant activity of various extracts (20, 40, 60, and 80 µg/ml). In an ethanol solution, the samples reacted with stable DPPH radicals. The reaction mixture was composed of 0.5 ml of the sample, 3 ml of absolute ethanol, and 0.3 ml of DPPH radical solution in 0.5 ml of ethanol. The DPPH radical is reduced when it interacts with hydrogen-donating antioxidants. After 100 min of processing, the hue shift (from deep violet to light yellow) was measured at 517 nm. The blank was a combination of ethanol (3.3 ml) and the sample (0.5 ml). Ethanol (3.5 ml) and DPPH radical solution (0.3 ml) were combined to prepare the control solution. The percentage of scavenging activity of the antioxidant activity was determined using equation (1):

$$\text{DPPH scavenging activity \%} = \frac{(A_{Control}) - (A_{Sample})}{(A_{Sample})} \times 100$$

Control=control absorption (without antioxidant), Sample=absorption after addition of biosynthesized TiO_2 Nanoparticles for each concentration

2.5 Characterization Techniques

X-ray diffraction (XRD) was used to examine the crystal structure and phase purity of the produced nanoparticles (PANalytical X'Pert PRO diffractometer). A Perkin Elmer spectrophotometer was used to record FTIR spectra in the 400–4000 cm^{-1} range to identify the surface functional groups. A LABINDIA UV 3092 spectrophotometer was used to acquire UV–visible diffuse reflectance spectra in the 200–800 nm wavelength range. The surface morphology and elemental composition were investigated using scanning electron microscopy (SEM) and energy-dispersive X-ray spectroscopy (EDS; Quanta FEG-200). The size, shape, and crystallinity of the particles were examined using high-resolution transmission electron microscopy (HR-TEM; JEOL JEM-2100 Plus). For the DPPH radical scavenging activity experiment, the absorbance at 517 nm was measured using a UV-Vis spectrophotometer (UV-10, Thermo).

3 Results and discussion

3.1 X-Ray Diffraction Analysis

X-ray diffraction analysis was used to analyze the crystalline structure, phase composition, and average crystallite size of the chemically synthesized TiO_2 (C-TiO_2), green-synthesized TiO_2 (G-TiO_2), and Ba-doped biosynthesized TiO_2 nanoparticles. Figure 2 shows the XRD patterns of each sample. The formation of a tetragonal TiO_2 crystal structure was confirmed by the diffraction angles (2θ) at 25.62°, 37.26°, 38.10°, 48.35°, 54.16°, 55.36°, 62.41°, 68.99°, 70.54°, and 75.28°, which correspond to the Bragg reflection planes of anatase TiO_2.The obtained diffraction patterns show excellent agreement with the standard JCPDS card No. 89-4921, indicating high phase purity without detectable impurities [23].Compared to C-TiO_2,G-TiO_2 exhibited slightly broader diffraction peaks, suggesting a reduction in the crystallite size induced by phytochemical capping from the plant extract. In the case of Ba-doped TiO_2

nanoparticles, additional weak diffraction peaks appeared at $2\theta = 31.55^{\circ}$, 38.67°, 44.71°, 56.14°, 65.91° and 75.12°, which corresponded to the (110), (111), (200), (211), (220) and (310) planes of the cubic Ba-related phases, in accordance with JCPDS card No. 75-0461 [24]. The absence of secondary impurity phases indicates the successful incorporation of Ba^{2+} ions into the TiO_2 lattice and their uniform dispersion within the host matrices. A slight shift in the peak positions and variation in the peak intensities were observed for the Ba-doped TiO_2 sample, which can be attributed to the lattice distortion caused by the substitution of Ti^{4+} ions (ionic radius ≈ 0.61 Å) with larger Ba^{2+} ions (ionic radius ≈ 1.35 Å). This lattice strain plays a crucial role in modulating the electronic structure and charge carrier dynamics of TiO_2. The average crystalline size was calculated using Debye- Scherrer's formula

$$\mathrm{D} = \frac{K\,\lambda}{\beta\ COS\ \theta}$$

The average crystalline size of C-TiO_2 average crystallite size was approximately 37 nm of C-TiO_2 was 20 nm for G-TiO_2, and in the range of 20–25 nm for Ba-doped TiO_2 nanoparticles. The reduced crystallite size of the green-synthesized samples enhanced the surface-to-volume ratio, which is favorable for photocatalytic reactions.

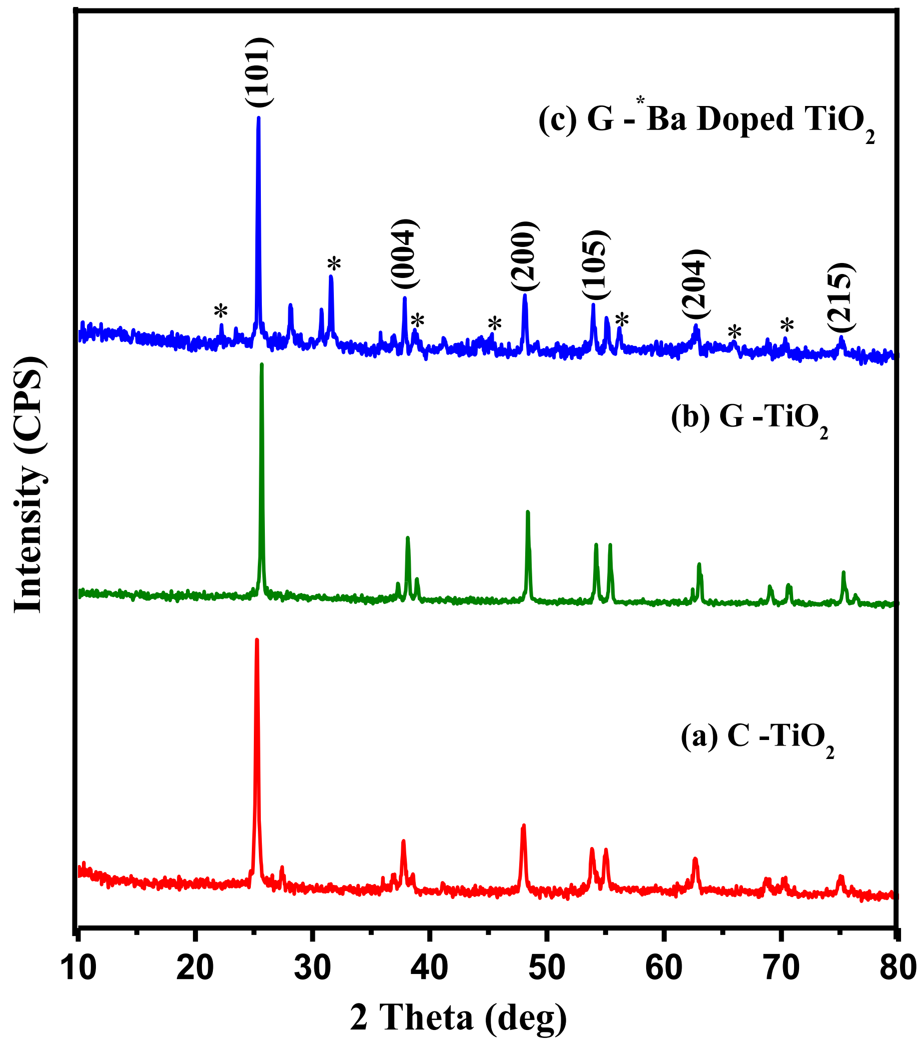

Fig. 2 XRD pattern of C-TiO_2, G-TiO_2 and G-Ba doped TiO_2 nanoparticles

3.2 UV–Visible spectroscopy

The optical behavior of the C-TiO_2, G-TiO_2, and G-Ba-doped TiO_2 nanoparticles was examined using UV–visible reflectance spectroscopy. The UV-visible reflectance spectra of C-TiO_2, G-TiO_2, and G-Ba-doped TiO_2 nanoparticles are displayed in Fig. 3 (a), with maximum reflectance at 354, 373, and 382 nm, respectively.

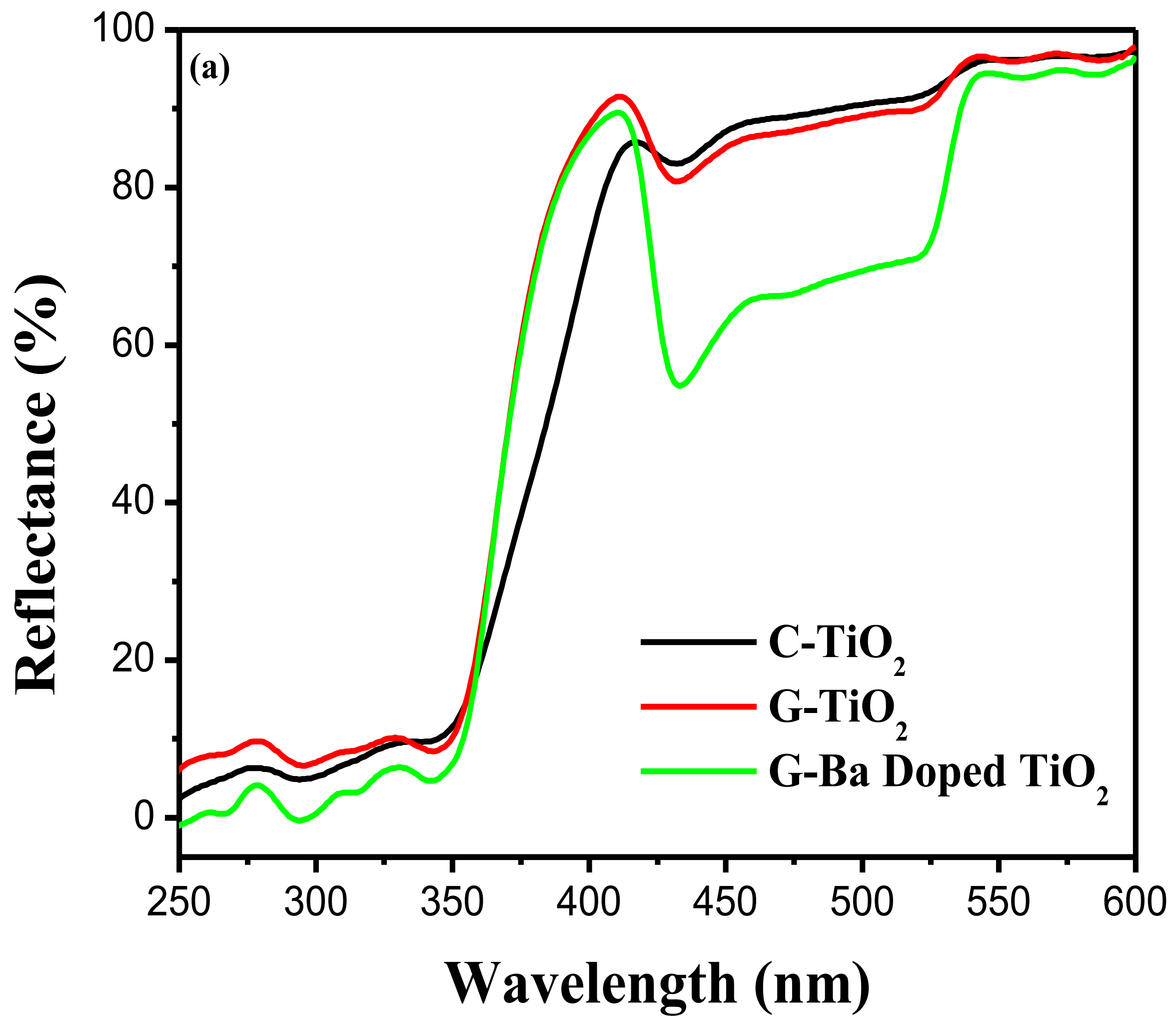

Fig. 3 (a) UV-Vis spectra of C-TiO_2, G-TiO_2, and G-Ba-doped TiO_2 nanoparticles

The reflectance and photon energy in the high-energy part of the absorption are related to the optical energy bandgap by the following equation:

$$E_g = \frac{hc}{\lambda} \text{ eV}$$

C-TiO_2, G-TiO_2, and G-Ba-doped TiO_2 were found to have band gap energies of 3.5, 3.32, and 3.24 eV, respectively.

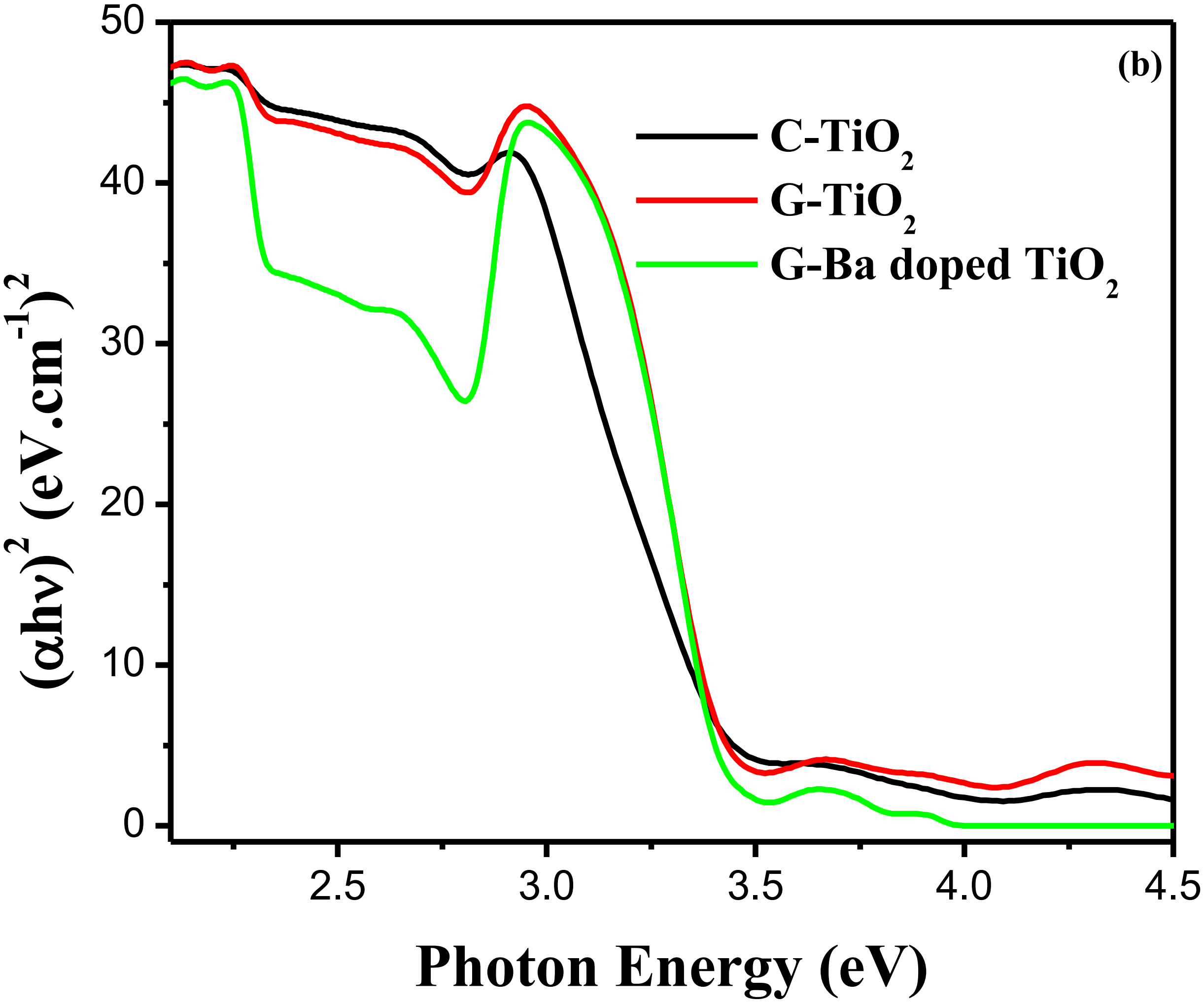

Fig.3 (b) Band Gap curve (Tauc plot) of C-TiO_2, G-TiO_2 and G-Ba doped TiO_2 nanoparticles

The $(\alpha h\nu)^2$ tauC plot against the photon energy hν is displayed in Fig. 3(b). The Eg values of C-TiO_2, G-TiO_2, and G-Ba doped TiO_2 nanoparticles were determined to be 3.5 eV, 3.3 eV, and 3.2 eV, respectively, by expanding the linear areas. Lattice distortion, size reduction, and surface modification with phytochemicals are linked to the little rise in bandgap energy with Ba doping and green synthesis. Together, these factors affect charge carrier mobility and reduce electron-hole recombination, which improves photocatalytic performance. [25].

3.3 Fourier Transform Infrared Spectroscopy

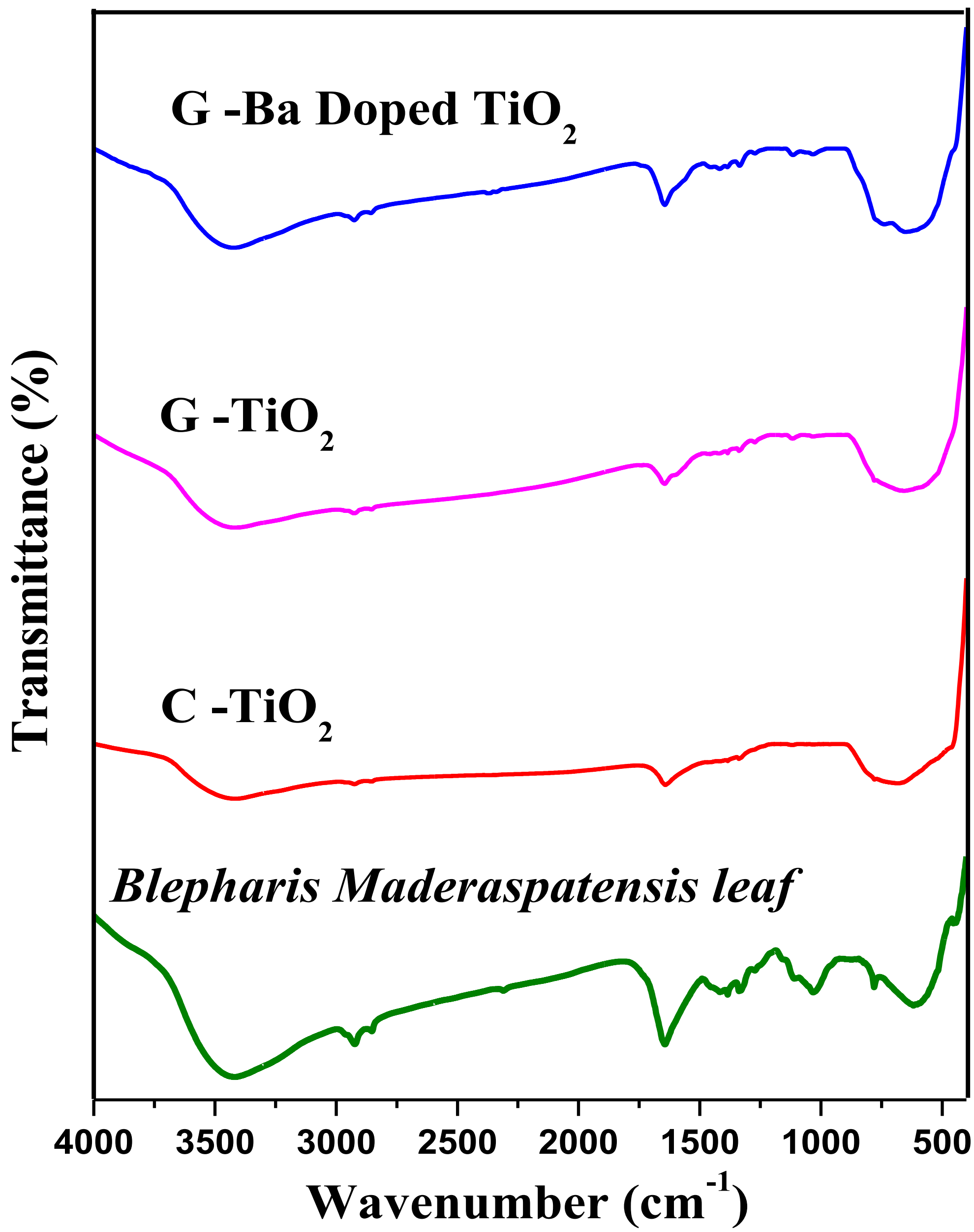

Fig. 4 FTIR spectra for C-TiO_2, G-TiO_2 and G-Ba doped TiO_2 nanoparticles

FTIR spectroscopy was used to identify the biomolecules that capped the bioreduced TiO_2 and Ba-doped TiO_2 nanoparticles generated using *Blepharis maderaspatensis* leaf extract (Fig. 4). The O–H stretching of alcohol was represented by a prominent peak in the FT-IR spectra of the leaf extract at 3416 cm^{-1}, whereas the C–H stretching vibrations of alkyl and aldehyde groups were represented by peaks at 2923 cm^{-1} and 2852 cm^{-1}, respectively. A clear, very strong absorption band at 1644 cm^{-1} was identified as amide due to the carbonyl bending vibrations in the amide linkages of the proteins in the extract. The peaks at 1417 cm^{-1} were indicative of the bending vibrations of the CH functional groups. The peaks at 1384 cm^{-1} and 1032 cm^{-1} are attributed to the C–N stretching vibrations of aromatic and aliphatic amines, respectively. The band at 879cm^{-1} is thought to show the bending vibrations of the C–H groups of the phenyl rings. The presence of an aromatic C-H group is associated with a peak at 618cm^{-1} [26].The O-H stretching caused by the alcoholic group is shown by the peak at 3417cm^{-1} in the FTIR spectra of TiO_2 nanoparticles, whereas the distinctive peak of the N–H bent bond is represented by the band at 1641cm^{-1} [27]. The vibration of the Ti-O-O bond was reflected by the peaks at 779cm^{-1} and 679cm^{-1} [28]. The FTIR spectra of the G-TiO2 and G-Ba-doped TiO_2 nanoparticles showed the typical C = C bonds at 1645 cm^{-1} for asymmetric carboxylic vibrations. The G-TiO_2 nanoparticles displayed a peak at 1418 cm^{-1} for symmetric carboxylic vibrations. These peak shifts indicate that the *Blepharis maderaspatensis* extract was incorporated into the nanoparticles. For G-TiO_2 and Ba-doped TiO_2 nanoparticles, the O-H stretching is observed at 3412 cm^{-1}, and the peaks at 779 cm^{-1} and 658 cm^{-1} indicate the presence of Ti-O-Ti. This contributes to the photocatalytic activity of the nanoparticles, guaranteeing the successful synthesis of titanium dioxide nanoparticles utilizing leaf extract. They ensured the successful creation of titanium dioxide nanoparticles using leaf extract and contributed to the photocatalytic activity of these nanoparticles.

3.4 Scanning Electron Microscopy with Energy-Dispersive X-ray Spectroscopy

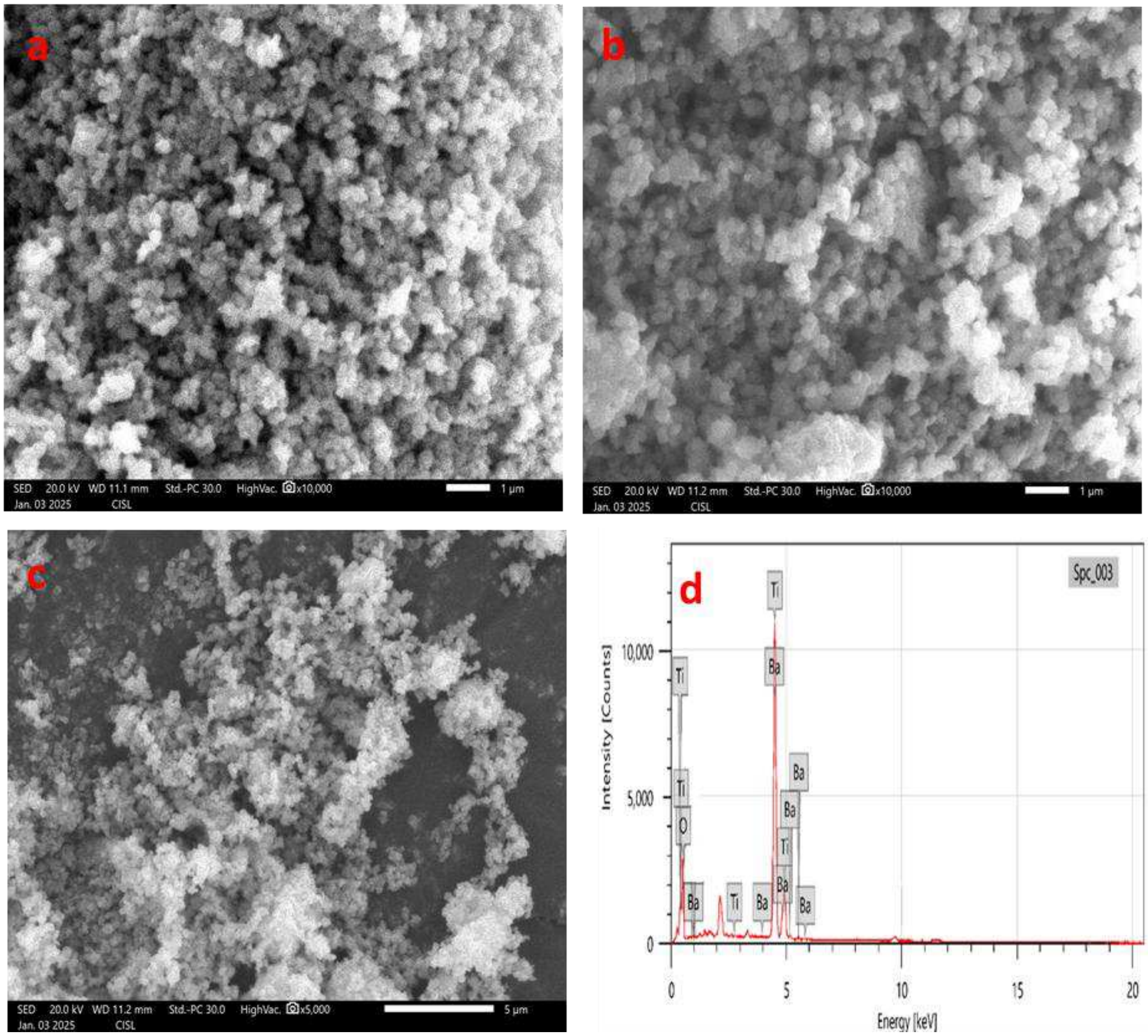

Fig. 5 SEM (a) C-TiO_2 (b) G-TiO_2 (c) G-Ba doped TiO_2 & (d) EDAX images of G-Ba doped TiO_2 nanoparticles

The surface morphologies of the chemically synthesized TiO_2, green-synthesized TiO_2, and green-synthesized Ba-doped TiO_2 nanoparticles were examined using scanning electron microscopy, as shown in Fig. 5. The chemically synthesized TiO_2 nanoparticles exhibited noticeable agglomeration with irregular particle distribution, which can be attributed to the absence of surface-stabilizing agents during the synthesis. In contrast, the green-synthesized TiO_2 nanoparticles displayed a relatively uniform and quasi-spherical morphology with reduced agglomeration, indicating the effective capping action of the phytochemicals present in the *Blepharis maderaspatensis* leaf extract [29]. Notably, the Ba-doped green-synthesized TiO_2 nanoparticles exhibited a more homogeneous distribution with well-defined spherical features and smoother surfaces. The average particle size, estimated from the SEM micrographs, was found to be in the range of 20–40nm, which is consistent with the crystallite sizes obtained from the XRD analysis. The observed reduction in particle size upon green synthesis and Ba incorporation can be ascribed to the combined influence of phytochemical capping and dopant-induced crystal growth inhibition.

Energy-dispersive X-ray spectroscopy was employed to confirm the elemental composition and purity of the synthesized nanoparticles. The EDS spectrum of Ba-doped TiO_2 nanoparticles (Fig. 4d) revealed the presence of Ti, O, and Ba without any detectable impurity elements, confirming the successful incorporation of Ba into the TiO_2 matrix. Weight and atomic percentage analyses further substantiated the homogeneous distribution of Ba dopants within the TiO_2 lattice. The enhanced surface area and abundance of active sites observed in Ba-doped TiO_2 nanoparticles are expected to promote efficient charge transfer and contribute significantly to their superior photocatalytic performance [30].

3.5. High Resolution Transmission Electron Microscopy (HR-TEM)

High-resolution transmission electron microscopy was employed to gain deeper insight into the morphology, particle size distribution, and crystallinity of the C-TiO_2, G-TiO_2, and Ba-doped G-TiO_2 nanoparticles, as illustrated in Fig.6–8. HR-TEM images revealed that the chemically synthesized TiO_2 nanoparticles possessed comparatively larger particle sizes with partial agglomeration. In contrast, the green-synthesized TiO_2 and Ba-doped TiO_2 nanoparticles predominantly exhibited quasi-spherical morphologies with improved dispersion and reduced particle size. The average particle sizes estimated from the TEM histograms were approximately 32 nm for C-TiO_2, 19 nm for G-TiO_2, and 21 nm for Ba-doped G-TiO_2 nanoparticles. The noticeable size reduction in the green-synthesized samples confirms the crucial role of plant-derived phytochemicals in regulating nucleation and growth processes during nanoparticle formation. Furthermore, Ba doping slightly increased the particle size compared to undoped G-TiO_2, which can be attributed to the lattice distortion and localized structural rearrangements induced by the larger Ba^{2+} ions. The selected-area electron diffraction (SAED) patterns exhibited distinct concentric rings corresponding to the (101), (200), and (220) planes of anatase TiO_2, confirming the polycrystalline nature and high crystallinity of all the samples. The absence of additional diffraction rings further supports the phase purity of the synthesized nanoparticles. The HR-TEM and SAED results were in excellent agreement with the XRD findings, validating the successful green synthesis and structural integrity of the Ba-doped TiO_2 nanoparticles.

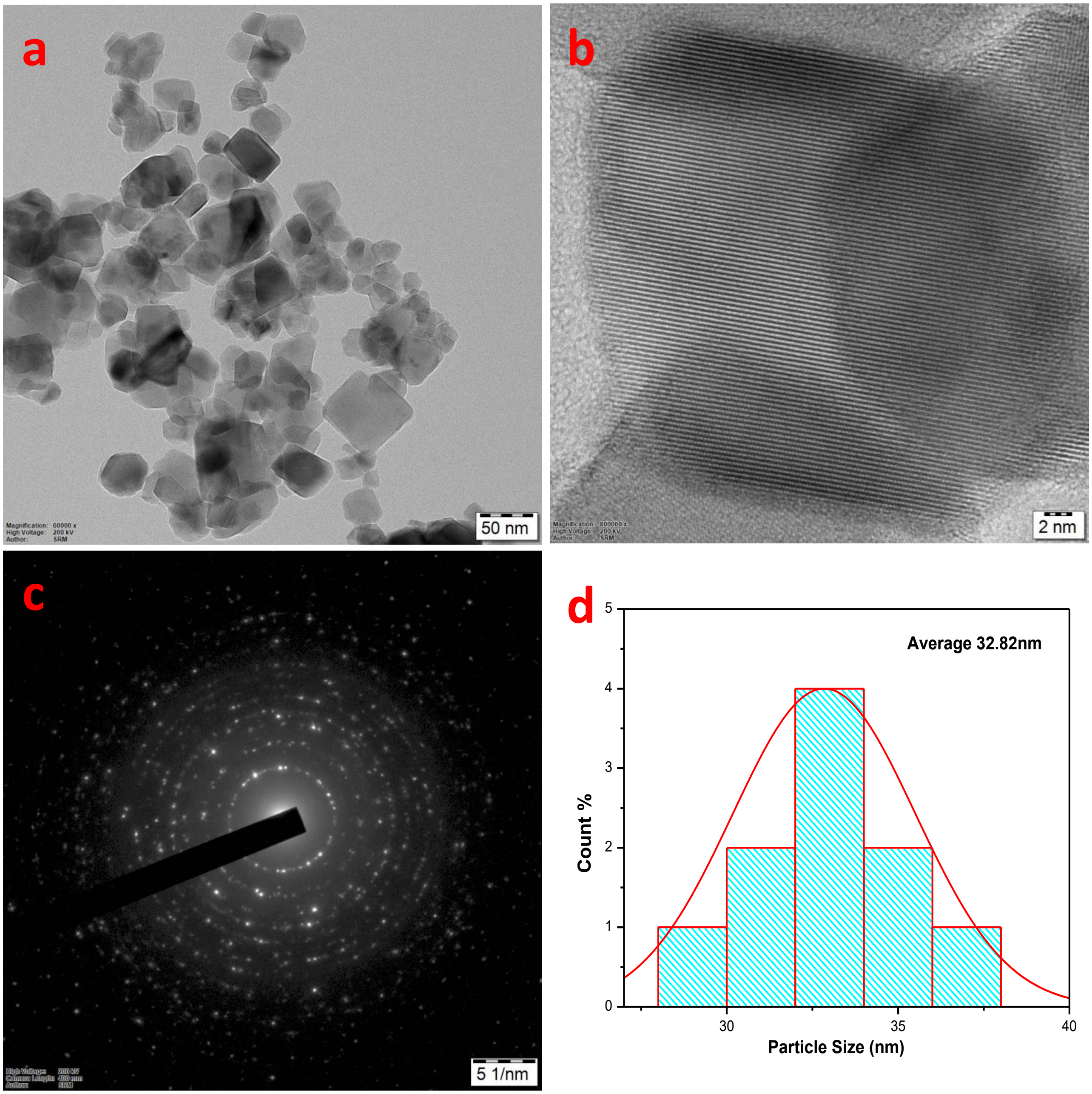

Fig. 6(a) TEM, (b) HRTEM images (c) SAED of C-TiO_2 and (d) Particle size histogram of C-TiO_2 nanoparticles

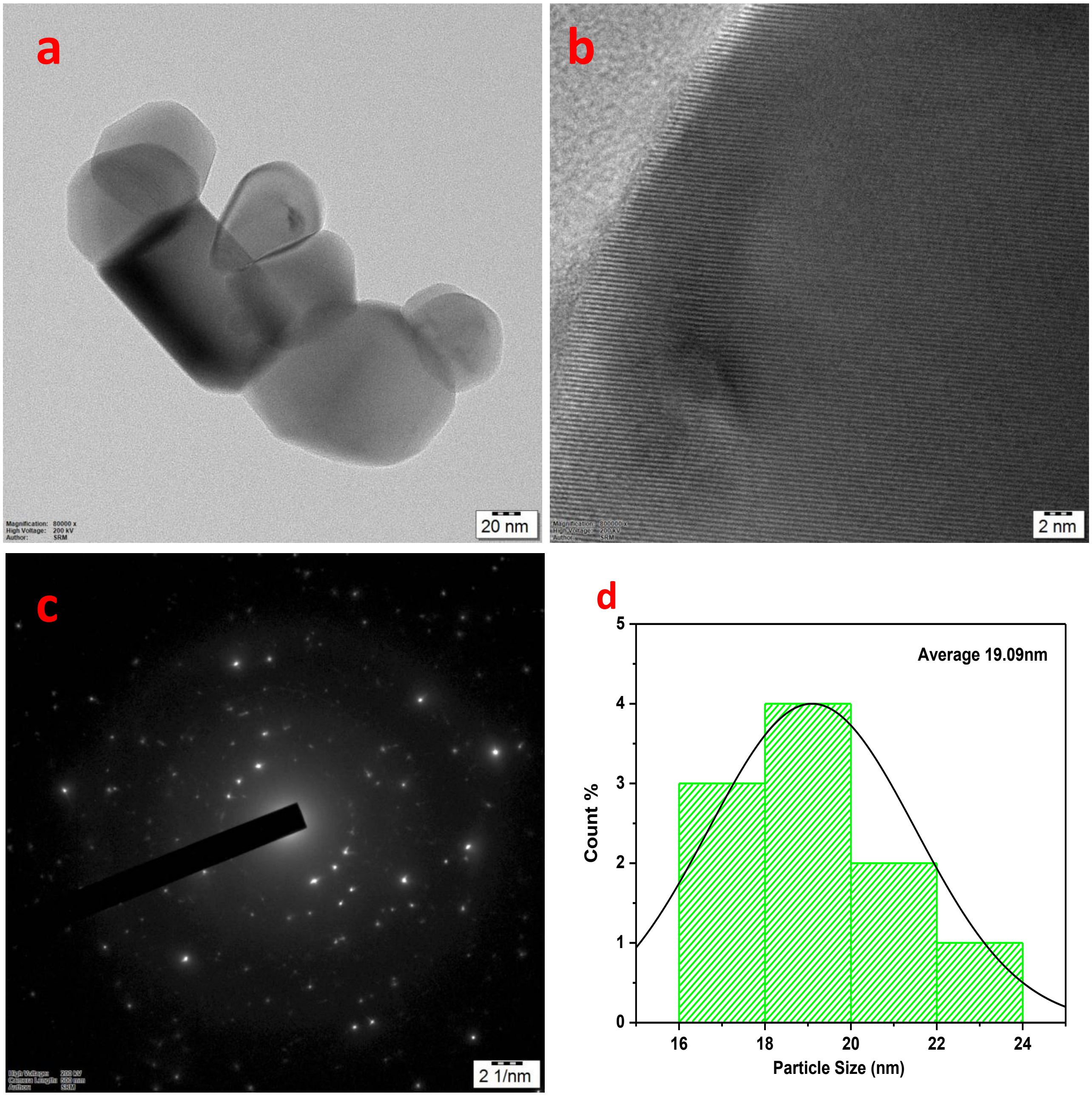

Fig. 7(a) TEM, (b) HRTEM images (c) SAED of G-TiO_2 and (d) Particle size histogram of G-TiO_2 nanoparticles

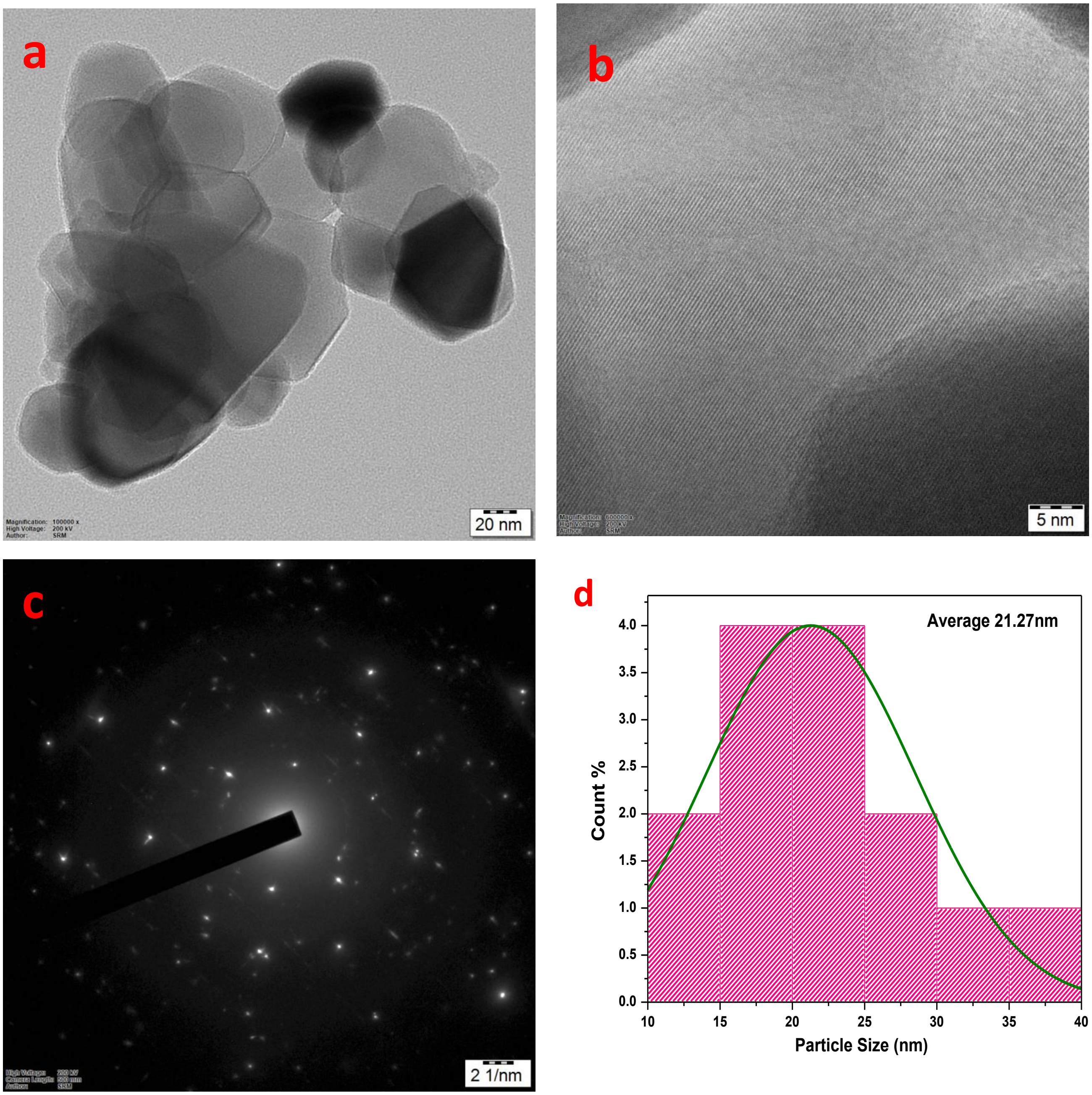

Fig. 8 (a) TEM, (b) HRTEM images (c) SAED of G-Ba doped TiO_2 and (d) Particle size histogram of G-Ba doped TiO_2 nanoparticles

3.6 Photocatalytic Activity

UV-visible irradiation was used to investigate the photodegradation of methylene blue dye. The photodegradation of methylene blue is depicted schematically in Figures 9–11. The following formula was used to determine the TiO_2 nanoparticles photodegradation efficiency:

$$\text{Degradation } (\%) = (C_0 - C_t) / C_0 \times 100$$

Where C_0 is the initial concentration of MB, and C_t is the temporal concentration of MB at time t [32]. The photocatalytic activities of chemically and biomedically mediated TiO_2 Nanoparticles and Ba-TiO_2 Nanoparticles were evaluated using methylene blue. As methylene blue dye is frequently used in the textile industry for coloring and is more dangerous to people, it was used as a pollutant in this study. Thus, the removal of methylene blue from wastewater is challenging [33]. The methylene blue dye absorption spectra and photodegradation efficiency were measured at regular intervals. The UV absorption spectra of methylene blue at 664 nm correspond to the π–π^* transition. Methylene blue deteriorates, according to the results of the absorption peak intensity reduction. Compared to chemically and environmentally synthesized TiO_2 Nanoparticles, biologically produced Ba-TiO_2 Nanoparticles have higher degradation efficiency. The degradation efficiency of the jasmine flower extract was improved by the hydroxyl group. The maximum degradation of bio-mediated Ba-TiO_2 Nanoparticles less than 100 min of exposure was 96%.

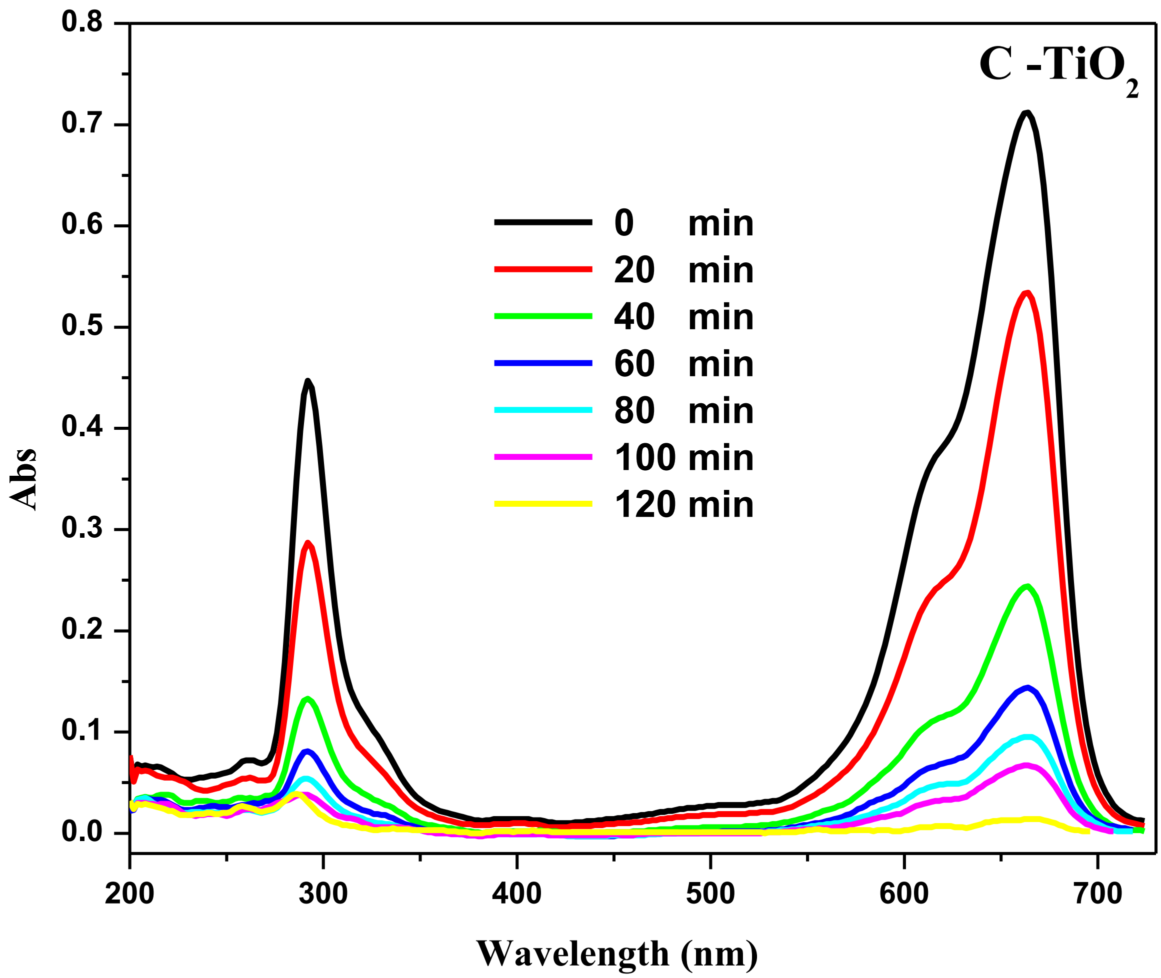

Fig. 9 UV–visible spectra of methylene blue degradation of C-TiO_2 nanoparticles

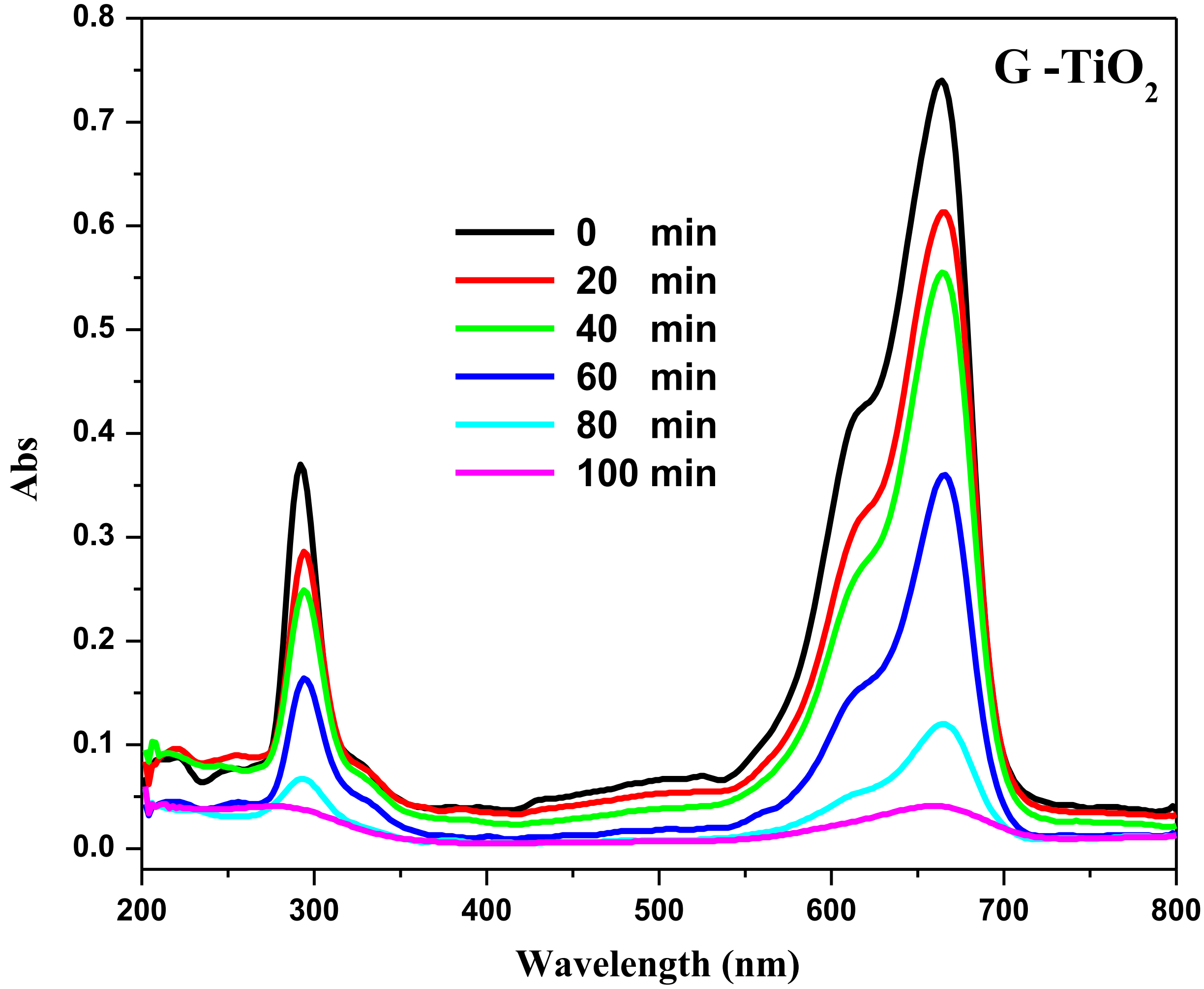

Fig. 10 UV–visible spectra of methylene blue degradation of G-TiO_2 nanoparticles

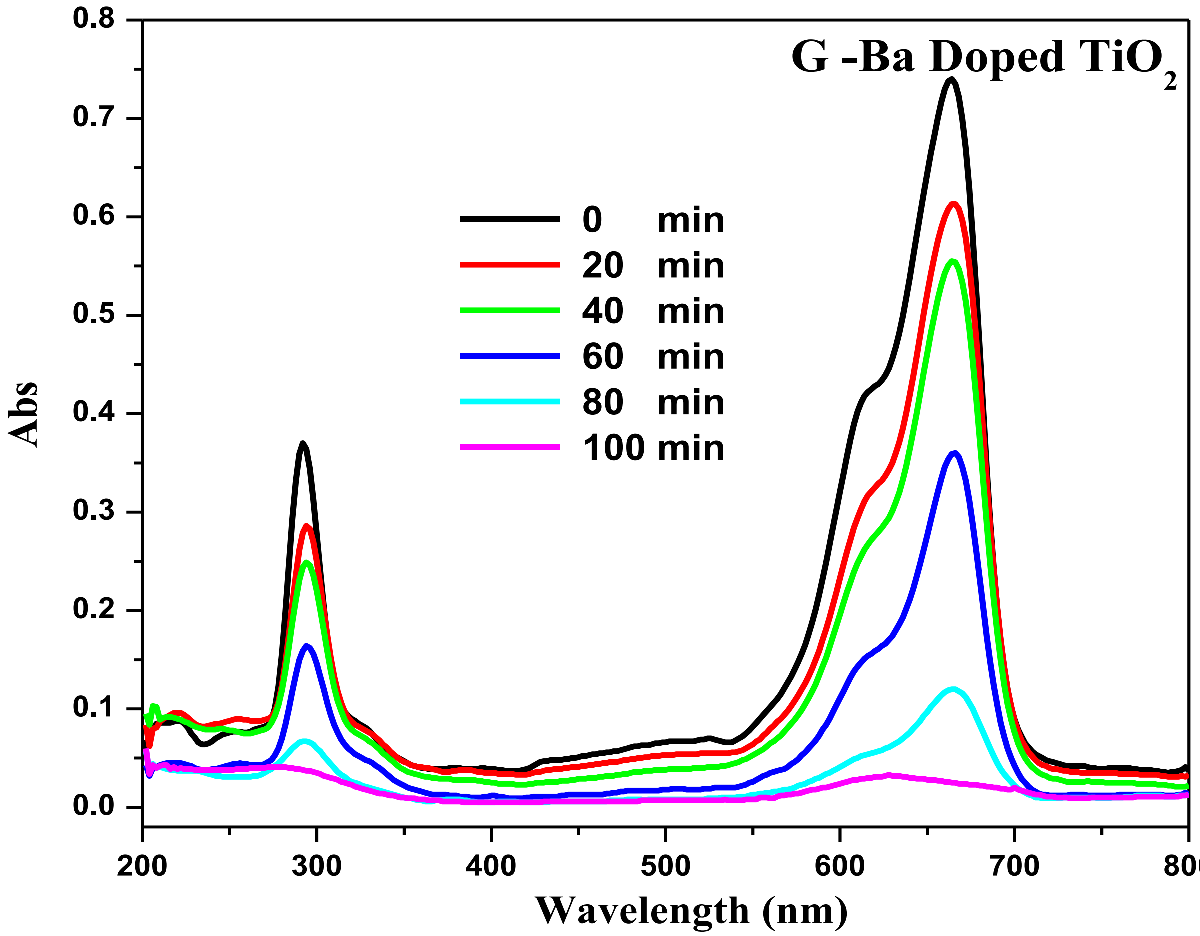

Fig.11 UV–visible spectra of methylene blue degradation of G-Ba doped TiO_2 nanoparticles

Mechanism

In the context of MB dye, a hole (h^+) operates as a dominant scavenger, whereas an electron acts as a substantial scavenger, according to the previously reported experimental study. To put it another way, MB dye demonstrates that electrons are primarily responsible for scavenging radicals. This suggests that donating electrons to neutralize radicals is more likely. Holes in the MB dye dominate the radical scavenging mechanism. This result implies that it is more likely to require electrons to combat radicals.

Additionally, the presence of both existing and stabilized electrons and holes resulted in a greater number of radicals, as shown by the mechanism presented in Eqs. (1), (2), (3), (4), (5), (6), and (7).

(1) C-TiO_2 Nanoparticles + G-TiO_2Nanoparticles + G-Ba-TiO_2 Nanoparticles + hv → G-TiO_2 (Ba^{2+}) Nanoparticles* + e^{-}_{CB} + h_{VB}^{+}

(2) H_2O + h_{VB}^{+} → H+ +$OH^{\bullet}$

(3) O_2 + e_{CB}^{-} → O_2^{-}

(4) OH^{-} + h^{+} → $OH^{\bullet}$

(5) O_2 + 2H + $2e^{-}$→H_2 + O_2^{-}

(6) H_2O_2 + e^{-}→ OH^{-} +$OH^{\bullet}$

(7) MB + OH• or h^{+}→   Degradation products

When radiation with energy equal to or higher than the band gap energy strikes TiO_2 particles, O_2^{-} represents the superoxide radical adsorbed on the surface of the catalyst particles, and e^{-} C**B**+ h^{+} VB represents the photoexcited electrons in the conduction band (CB) and holes in the valence band (VB), respectively [34–36]. The generation of photoexcited charge carriers and the ensuing redox reactions that propel the degradation of the MB dye are depicted in Figure 12.

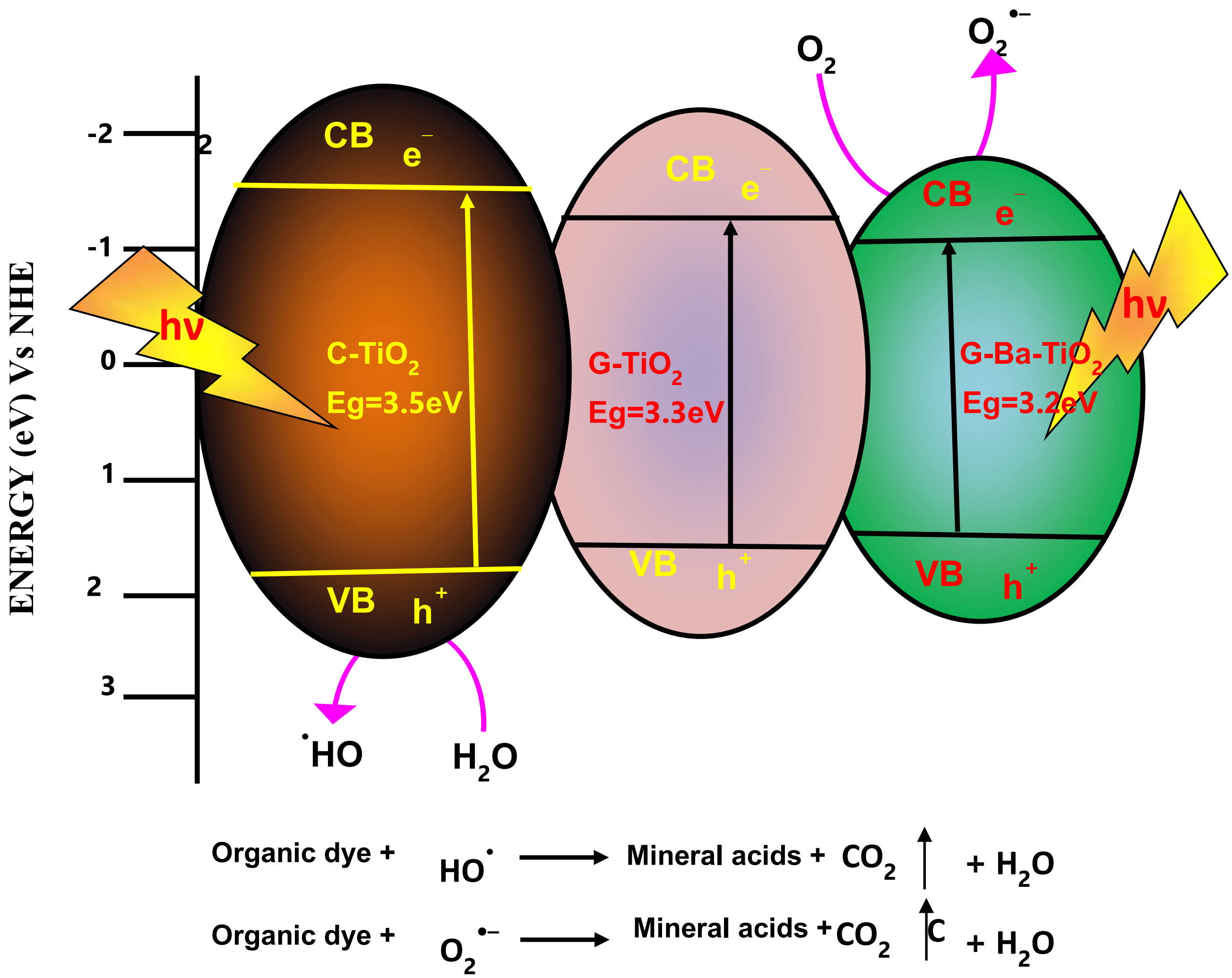

Fig. 12 Schematic diagram of Methylene blue dye degradation process

An electron-hole pair was produced when UV-visible light was applied to the C-TiO_2, G-TiO_2, and G-Ba-TiO_2 nanoparticles. G-Ba-TiO_2 nanoparticles positive holes split water molecules into hydrogen gas and free radicals, while their negative electrons combine with oxygen molecules to create superoxide anions. Superoxide ($O_2^{\bullet-}$) and hydroxyl groups ($OH^{\bullet}$) are produced by electron–hole pairs. These superoxide and hydroxyl groups break down methylene blue.

Methylene blue is converted to Leuco methylene blue (LMB) during the reduction process (Figure 12). The bio-mediated Ba-TiO_2 nanoparticles, bio-mediated TiO_2, and chemically synthesized TiO_2 nanoparticles exhibited degradation efficiencies of 96%, 82%, and 81%, respectively.

3.7Antioxidant Activity

An antioxidant test based on electron transfer, the DPPH (2, 2-diphenyl-1-picryl-hydrazyl-hydrate) free radical method, produces a violet solution in ethanol. The capacity of the biosynthesized TiO_2 nanoparticles to scavenge free radicals was examined in relation to DPPH free radicals [37]. The antioxidant effectiveness of the produced TiO_2 Nanoparticles is shown in Fig. 13-14. Both the biosynthesized TiO_2 nanoparticles and the ethanol concentration utilized as a positive control were identical. TiO_2 and ethanol were used in varying amounts (20, 40, 60, and 80 µg/mL). At a concentration of 80µg/mL, the green TiO_2 nanoparticles produced exhibited approximately 74.80% and 76.57% DPPH radical scavenging activity (Table 1-2). The phenolic components of phytochemicals on the surface of TiO_2 Nanoparticles produced using environmentally friendly techniques demonstrated a discernible antioxidant capability.

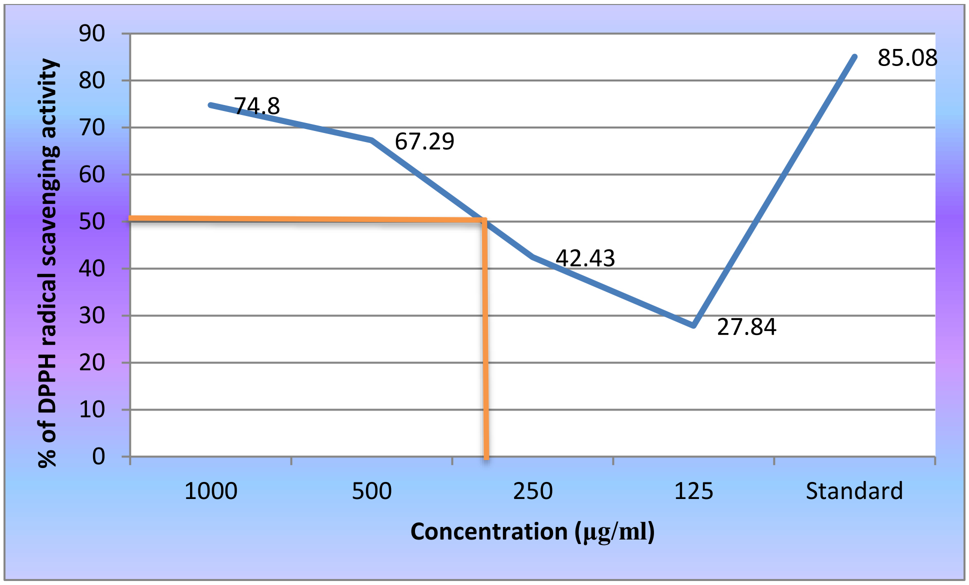

Fig. 13 Antioxidant activity of G-TiO_2 for Different Concentration

S.No	Concentration (µg/ml)	OD (517 nm)	% of DPPH activity
1	1000	0.228	**74.80**
2	500	0.341	**67.29**
3	250	0.521	**42.43**
4	125	0.653	**27.84**
5	Standard	0.135	**85.08**

Table 1 Antioxidant activity of G-TiO_2 for Different Concentration

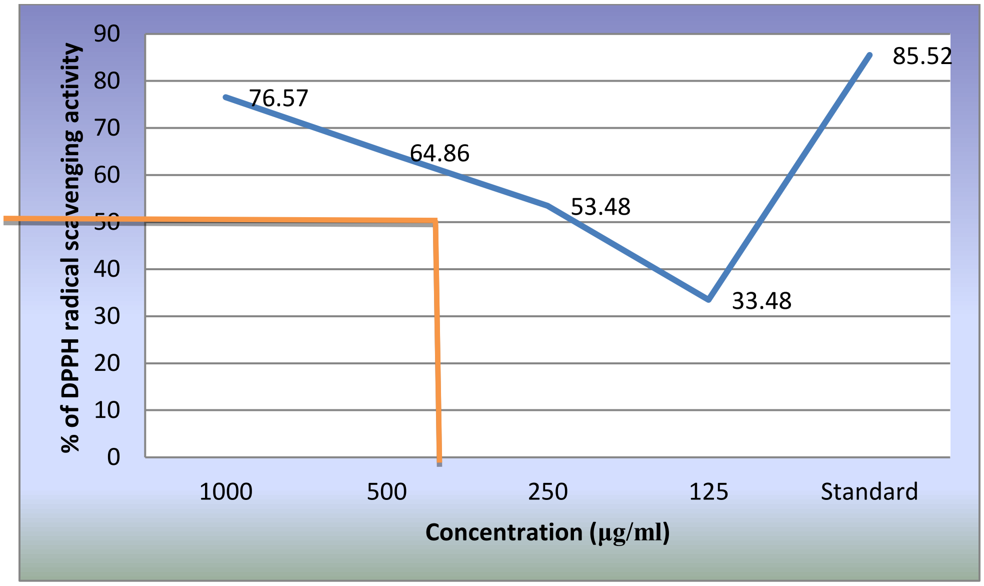

Fig. 14 Antioxidant activity of Ba-doped G-TiO_2 for Different Concentration

S.No	Concentration (µg/ml)	OD (517 nm)	% of DPPH activity
1	1000	0.212	**76.57**
2	500	0.318	**64.86**
3	250	0.421	**53.48**
4	125	0.602	**33.48**
5	Standard	0.131	**85.52**

Table 2 Antioxidant activity of Ba-doped G-TiO_2 for Different Concentration

4 Conclusion

In this study, C-TiO_2, G-TiO_2, and G-Ba-doped TiO_2 nanoparticles were successfully prepared using a hydrothermal technique with *Blepharis maderaspatensis* leaf extract. Structural, optical, functional, and morphological characterizations employing X-ray diffraction (XRD), UV-Vis spectroscopy, Fourier-transform infrared (FTIR) spectroscopy, scanning electron microscopy (SEM), energy-dispersive X-ray spectroscopy (EDS), and high-resolution transmission electron microscopy (HR-TEM) indicated the successful synthesis of C-TiO_2, G-TiO_2, and G-Ba-doped TiO_2 nanoparticles. According to the XRD examination, the ecologically generated material had a tetragonal structure (anatase phase) with an average crystal size between 20-40 nm. The bandgap energies of C-TiO_2, G-TiO_2, and G-Ba-doped TiO_2 nanoparticles increased following barium doping, according to the UV-Vis absorption spectra. FTIR analysis revealed the presence of O-Ti-O group bonds that could be adsorbed on G-Ba-doped TiO_2 nanoparticles. However, the SEM study showed that the morphology was agglomerated and spherical. Under UV-visible light, methylene blue undergoes photodegradation. Biomedicated TiO_2 showed a maximum degradation efficiency of 96% after 100 min of exposure. For use in wastewater treatment and biomedical industries, G-Ba-doped TiO_2 nanoparticles were found to be more efficient photocatalysts than C-TiO2 nanoparticles. Furthermore, the strong capacity of the biosynthesized TiO_2 nanoparticles to scavenge free radicals was confirmed by the antioxidant potential evaluated using DPPH tests. Furthermore, the strong capacity of the biosynthesized TiO_2 nanoparticles to scavenge free radicals was corroborated by the antioxidant potential evaluated using the DPPH assay.

Author contribution

M.Anbuvannan: Writing – original draft, Methodology, interpreted the data. V.Maria Vinosel, S.Rajesh: Writing – review & editing. P.Dhatshanamurthi, Karuppaiah Selvakumar: Software, Formal analysis. D.Lakshmanan, M.Ramesh,: Visualization, Computational resources. Aboud Ahmed Awadh Bahajjaj, Mohamed Ouladsmane: Methodology, Funding acquisition, Formal analysis.

Data availability Data will be made available on request.

Declarations

Ethics Statement Not applicable.

Competing interests The authors declare no competing interests.

Acknowledgement

This work was funded by the ongoing Research Funding Program Number (ORF-2026-763), King Saud University, Riyadh, Saudi Arabia.

References

1. S. Shekhar , S.Singh , N.Gandhi , S.Gautam , B. Sharma. Green chemistry based benign approach for the synthesis of titanium oxide nanoparticles using extracts of *Azadirachta Indica.* Cleaner Eng.and Tech. **13**, 100607 (2023)
2. S.Subhapriya , P.Gomathipriya . Green synthesis of titanium dioxide (TiO_2) nanoparticles by *Trigonella foenum-graecum* extract and its antimicrobial properties. Micro.Pathogen.**116**, 215–220, (2018)

3. G.Nabi , Q.Ul- Ain , M. Bilal Tahir , K. Nadeem Riaz , T. Iqbal, M. Rafique, S.Hussain, W.Raza, I. Aslam and M. Rizwan. Green synthesis of TiO_2 nanoparticles using *lemon peel* extract: their optical and photocatalytic properties. Inter. J. of Enviro. Analyti.Chem. 102(2),434-442 ,(2020)
4. V.Helan, JJ. Prince, NA. Al-Dhabi, MV. Arasu, A. Ayeshamariam, G Madhumitha, SM. Roopan, M. Jayachandran . *Neem* leaves mediated preparation of NiO nanoparticles and its magnetization, coercivity and antibacterial analysis. Results Phys. **6**,712–718, (2016)
5. I. Hussain, NB. Singh, A. Singh, H. Singh, SC. Singh. Green synthesis of nanoparticles and its potential application. Biotech Lett. **38**(4),545–560, (2016)
6. G. Nabi, W. Raza, MB. Tahir .Green synthesis of TiO_2 nanoparticle using cinnamon powder extract and the study of optical properties. J. Inorg. Organomet. Polym. Mater **30**(4),1425–1429,(2020)
7. MV. Arularasu Effect of organic capping agents on the optical and photocatalytic activity of mesoporous TiO_2 nanoparticles by sol–gel method. SN App.Sci. **1**(5),393,(2019)
8. JM. Abisharani, S. Devikala, RD Kumar, M. Arthanareeswari, P. Kamaraj Green synthesis of TiO_2 nanoparticles using Cucurbita pepo seeds extract. Mat. Today Proc. **14**,302–307,(2019)
9. C. Ragupathi, JJ. Vijaya, S. Narayanan, LJ. Kennedy, S. Ramakrishna. Catalytic properties of nanosized zinc aluminates prepared by green process using Opuntiadilenii haw plant extract. Chin J Catal **34**(10),1951–1958 (2013)
10. S. Sikaria, S. Chitra, G. Dhanraj, R. Ramasubburayan. Vitex negundo leaf extract-assisted synthesis of TiO_2 nanoparticles and deciphering its in vitro antibacterial, antibiofilm, cytotoxic and anti-migratory activities, Materials Let. 403, 139460 (2026)

11. SA. Patil, DV. Shinde, DV. Patil, KK. Tehare, VV. Jadhav, JK. Lee, RSNK. Mane-Shrestha, SH. Han A simple, room temperature,solid-state synthesis route for metal oxide nanostructures. J. Mater. Chem. A **2**(33),13519–13526 (2014)
12. RK. Chava, M. Kang. Improving the photovoltaic conversion efficiency of ZnO based dye sensitized solar cells by indium doping. J. Alloy Compd. **692**,67–76 (2017)
13. M.Reinke, E.Ponomarev, Y.Kuzminykh, P.Hoffmann. Combinatorial characterization of TiO_2 chemical vapor deposition utilizing titanium isopropoxide. ACS. Comb. Sci. **17**(7),413–420 (2015)
14. M. Stucchi, CL. Bianchi, C. Argirusis, V. Pifferi, B. Neppolian, G.Cerrato, DC. Boffito. Ultrasound assisted synthesis of Ag-decorated TiO_2 active in visible light. Ultrason. Sonochem. **40**,282–288 (2018)
15. D. Devipriya, SM. Roopan. Cissus quadrangular is mediated ecofriendly synthesis of copper oxide nanoparticles and its antifungal studies against Aspergillus Niger, Aspergillus flavus. Mater. Sci. Eng. C **80**,38–44 (2017)
16. K. Velayutham ,A.Abdul Rahuman , G. Rajakumar ,T. Santhoshkumar , S.Marimuthu ,C. Jayaseelan , A. Bagavan , A. Vishnu Kirthi ,C. Kamaraj , A. Abduz Zahir , G. Elango. Evaluation of Catharanthus roseus leaf extract-mediated biosynthesis of titanium dioxide nanoparticles against Hippobosca maculata and Bovicola ovis. Parasitol. Res. **111**,2329–2337 (2012)
17. T. Santhoshkumar, A. Abdul Rahuman, C. Jayaseelan,G. Rajakumar, S. Marimuthu, A. Vishnu Kirthi, K. Velayutham, J.Thomas, J.Venkatesan, S.K Kim. Green synthesis of titanium dioxide nanoparticles using Psidium guajava extract and its antibacterial and antioxidant properties. Asian Pac. J.of Trop. Med. **7** (12) 968-976 (2014)

18. W. Ahmad, K.Kumar Jaiswal, S. Soni. Green synthesis of titanium dioxide (TiO_2) nanoparticles by using Mentha arvensis leaves extract and its antimicrobial properties, Inorganic and Nano-Metal Chem.**50** (10) 1032-1038 (2020)

19. Y.Singh, H. Patel , A. Rai, S. Singh, N. Srivastav, P. Srivastava. Bio-capped synthesis of TiO_2 nanoparticle using Murraya koenigii leaf extract via ultrasonication assisted sol-gel method and its advanced DSSC performance. Next Mat. **8** 100680 (2025)

20. W. Agatha, K.Yano, K.Sato, E. Park, Y.Iso , T. Isobe. Musa AAA and Jatropha curcas L . sap mediated TiO_2 nanoparticles: Synthesis and characterization. Sci. African **6** e00203 (2019)

21. T.Santhoshkumar, A.A. Rahuman, C. Jayaseelan, G. Rajakumar, S. Marimuthu, A.Vishnu Kirthi, K.Velayutham, J. Thomas, J. Venkatesan, S.K. Kim.Green synthesis of titanium dioxide nanoparticles using Psidium guajava extract and its antibacterial and antioxidant properties. Asian Pacific J.of Trop. Med. **7**(12) 968-976 (2014)

22. R. Saini , P. Kumar. Green synthesis of TiO_2 nanoparticles using *Tinospora cordifolia* plant extract & its potential application for photocatalysis and antibacterial activity. Inorg. Chem. Com. **156** 111221 (2023)

23. D. Hariharan, A. Jegatha Christy, J. Mayandi , L.C. Nehru. Visible light active photocatalyst: Hydrothermal green synthesized TiO_2 Nanoparticles for degradation of picric acid Materials Let.**222** 45–49 (2018)

24. M. Anbuvannan ,V. Maria Vinosel ,P. Dhatshanamurthi , S. Rajesh , M. Ramesh ,N. Kannadasan.Investigation of pure TiO_2 and BaO-loaded TiO_2 nanocomposites with enhanced photocatalytic activities J Nanopart Res. **27**(49) 1-11 (2025)

25. M. Aravind,M. Amalanathan, M. Sony Michael Mary, Synthesis of TiO_2 nanoparticles by chemical and green synthesis methods and their multifaceted properties SN App. Sci. **3**:409 (2021)

26. M.Sundrarajan, K.Bama, M.Bhavani, S.Jegatheeswaran, S.Ambika, A.Sangili, P.Nithya, R. Sumathi . Obtaining titanium dioxide nanoparticles with spherical shape and antimicrobial properties using *M. citrifolia* leaves extract by hydrothermal method. J.of Photoche. & Photobiology, B: Biology. **171** 117-124 (2017)

27. A. Girigoswami , B. Deepika , A. Kumar Pandurangan and K. Girigoswami. Preparation of titanium dioxide nanoparticles from *Solanum Tuberosum* peel extract and its applications Artif. Cells, Nanomed.and Biotech. **52** (1) 59-68 (2024)

28. S. Pratap Goutama, G. Saxenab, V.Singhc, A. Kumar Yadava, R. Naresh Bharagavab, K. B. Thapaa. Green synthesis of TiO_2 nanoparticles using leaf extract of *Jatropha curcas L.* for photocatalytic degradation of tannery wastewater. Chem. Eng.J.**336** 386–396 (2018)

29. M.V. Reddy, R. Jose, T.H. Teng, B.V.R. Chowdari, S. Ramakrishna, Preparation and electrochemical studies of electrospun TiO_2 nanofibers and molten salt method nanoparticles, Electro. Acta **55** (9) 3109–3117(2010)

30. S. Mugundan , P. Praveen , S. Sridhar , S. Prabu , K. Lawrence Mary , Mohd Ubaidullah , S. F. Shaikh , S. Kanagesan. Sol-gel synthesized barium doped TiO_2 nanoparticles for solar photocatalytic application. Inorganic Chem. Comm.**139** 109340 (2022)

31. A. Mohanan Pillai, A. Harisankar, P. S. Salini , B.John, S. SarojiniAmma, Mercy Thelakkattu Devassy .Green synthesis of TiO_2 nanoparticles using *Beta vulgaris* extract and the evaluation of their photocatalytic and antibacterial activity. Ionics **30** 4257–4270 (2024)

32. S. Singh, GK. Sidhu, H. Singh. Removal of methylene blue dye using activated carbon prepared from biowaste precursor. Indian Chem.Eng **61**(1) 28–39(2019)
33. C. Parvathiraja, S. Shailajha, S. Shanavas, MK. Mubina .Photocatalytic and antibacterial activity of bio-treated Ag nanoparticles synthesized using *Tinospora cordifolia* leaf extract. J Mater Sci: Mater Electron **30**(9) 8515–8525(2019)
34. Yonas Etafa Tasisa , Tridib Kumar Sarma , Ramaswamy Krishnaraj , Suryakamal Sarma. Band gap engineering of titanium dioxide (TiO_2) nanoparticles prepared via green route and its visible light driven for environmental remediation. Results in Chemistry **11** 101850 (2024)
35. M Anbuvannan, V Maria Vinosel, P Dhatshanamurthi, M Ramesh, S Uvarajan. Structural, Optical and Photocatalytic Properties of $SrTiO_3$ Perovskite obtained by Solvothermal Method. Indian Journal of Pure & App.d Phy. **62** 423-428 (2024)
36. Ghulam Nabi , Abdul Majid , Asma Riaz , Thamer Alharbi , Muhammad Arshad Kamran ,Mansour Al-Habardi . Green synthesis of spherical TiO_2 nanoparticles using Citrus Limetta extract: Excellent photocatalytic water decontamination agent for RhB dye. Inorganic Chem.Com. **129** 108618 (2021)
37. Waseem Ahmad , Sanjay Kumar , Sarfaraz Ahmed, Microwave-assisted one-step biosynthesis of titanium dioxide nanoparticles: Antibacterial, antioxidant, and photocatalytic properties .Kuwait J. of Sci. **51** 100203 (2024)